Isolating the Contribution of the Koniocellular Visual Pathway in Aversive Learning in Human Visual Cortex

Abbreviated title: Koniocellular Contribution to Aversive Learning

Katherine J. McCain[1], Nathan M. Petro[2], and Andreas Keil[1]

[1]Department of Psychology,

University of Florida,

Gainesville, Florida 32603

[2]Institute for Human Neuroscience,

Boys Town National Research Hospital,

Boys Town, Nebraska 68010

Corresponding author: Katherine J. McCain, mccain.k@ufl.edu

Number of pages: 36
Number of figures: 7
Number of tables: 0
Number of words in abstract: 244
Number of words in significance statement: 90
Number of words in introduction: 614
Number of words in discussion: 1124

The authors declare no conflicts of interest.

Acknowledgments: This research was supported by grant R01MH125615 from the National Institutes of Health.

Abstract

The present study examined how the koniocellular retino-geniculate visual pathway contributes to the electrocortical amplification of threat cues in human visual cortex using a simple aversive conditioning task. The task involved S-cone isolating stimuli (Tritan condition) and achromatic luminance stimuli (luminance condition) that preferentially activated the koniocellular pathway and luminance channels, respectively. Steady-state visual evoked potential (ssVEPs) responses to the conditioned threat cues (CS+) and safety cues (CS-) in each condition were analyzed using a non-parametric Bayesian bootstrapped approach. The Tritan and luminance conditions exhibited greater ssVEP responses to the CS+ stimuli compared to the CS- stimuli in occipital sensors early into the trial (0 ms - 1000 ms; logBF10 > 2). In addition to these early conditioning effects, a late conditioning effect was observed (1500 ms - 2500 ms) in the Tritan condition that emerged over bilateral anterior sensors (logBF10 > 2). To further examine the koniocellular contribution to aversive learning, transitive Bayes factors were computed to compare the magnitude of the conditioning effects across conditions. Transitive Bayesian comparisons showed that the early conditioning effect was larger for the luminance condition than for the Tritan condition (logBF10 > 2). Furthermore, the late conditioning effect remained larger in the Tritan condition compared to the luminance condition (logBF10 > 2). Our results are consistent with previous work demonstrating that Tritan stimuli elicit enhanced electrocortical responses and with theoretical notions suggesting that the koniocellular pathway contributes to the representation of threat signals in human visual cortex.

Significance Statement

The functional roles of the koniocellular retino-geniculate pathway in human visual processing are topics of much interest. However, the extent that the koniocellular pathway contributes to the amplification of threat signals in the human visual cortex remains unclear. Therefore, the present study examined the contribution of the koniocellular pathway in aversive learning in humans using neurophysiological recordings. Our findings indicate that the koniocellular visual pathway plays a role in the electrocortical amplification of threat signals in humans and extends our growing understanding of the functional properties of the koniocellular pathway.

Isolating the Contribution of the Koniocellular Visual Pathway in Aversive Learning in Human Visual Cortex

Interactions between local inhibitory circuits in primary visual cortex (V1) and higher-order feedback projections are thought to contribute to the sharpening of excitatory lateral geniculate nucleus (LGN) afferents, facilitating the selective visuocortical amplification of motivationally relevant information (Angelucci et al., 2002; Keil et al., 2007; Briggs, 2020; Li and Keil, 2023). Several, electrophysiological studies have demonstrated that (Song and Keil, 2014; McTeague et al., 2015; Friedl and Keil, 2021) aversive conditioning resulted in heightened visuocortical responses to conditioned threat cues. These studies conveyed visual threat through luminance channels which primarily involve magnocellular and parvocellular retino-geniculate signals (Johnson et al., 2004). However, how the koniocellular retino-geniculate pathway contributes to the acquisition of aversive contingencies has yet to be established. Therefore, the present study aimed to investigate the koniocellular contribution to aversive learning in human visual cortex with a simple aversive conditioning paradigm.

Sparse cells in the koniocellular layers of the LGN receive blue-on yellow-off opponent color signals from small and large bistratified retinal ganglion cells and convey these signals to the superficial layers of V1 (Livingstone and Hubel, 1984; Hendry and Yoshioka, 1994; Hendry and Reid, 2000; Casagrande et al., 2007). Several studies have leveraged this color-opponent response property and have observed enhanced amplification of S-cone isolating signals despite the sparse distribution of cells in the koniocellular layers of the LGN (Cottaris and De Valois, 1998; Mullen et al., 2007, 2008; Horwitz, 2020). For instance, Mullen and colleagues (2008) identified a differential increase in BOLD activation in response to S-cone biasing stimuli: S-cone biasing stimuli prompted small BOLD responses at the level of the LGN, but strong

responses in V1. Therefore, based on this evidence, it is plausible that the koniocellular pathway is involved in the visuocortical amplification of S-cone biasing stimuli, and the enhancement of this signal may occur at the cortical level.

The koniocellular pathway exhibits neurophysiological connections to subcortical and deep cortical structures thought to be involved in the detection of salient visual information (Hendry and Reid, 2000; Nassi and Callaway, 2009; Huo et al., 2019). The superior colliculus, thought to be involved in the execution of ocular orienting to salient visual information, receives direct retinal input from the small and large bistratified retinal ganglion cells and exhibits afferents that project to the koniocellular layers of the LGN (Casagrande, 1994). Moreover, recent findings indicate that the inferior pulvinar nucleus of the thalamus, thought to be involved in higher-order visual processing, and the ventral koniocellular layer of the LGN are histologically continuous (Huo et al., 2019). Furthermore, the inferior pulvinar nucleus receives inputs from the superior colliculus and exhibits projections to V1 that are thought to contribute to the modulation of visuocortical activation (Stepniewska, 2003; Kaas and Lyon, 2007).

In the present study, we leveraged the properties of steady-state visual evoked potentials (ssVEPs) to measure selective visuocortical responses to conditioned threat (CS+) and safety cues (CS-). The koniocellular and luminance channel contributions to aversive learning were examined using S-cone isolating stimuli (Tritan condition; proposed by Cavanagh et al. 1992), and achromatic luminance stimuli (luminance condition), respectively. We expected the Tritan stimuli to elicit robust electrocortical responses, in line with several studies that observed substantial electrocortical activity in response to S-cone isolating stimuli (Cottaris and De Valois, 1998; Mullen et al., 2007, 2008; Horwitz, 2020). Furthermore, we expected greater ssVEP responses to the CS+ stimuli in both the luminance and Tritan conditions, compared to

the CS- stimuli (Song and Keil, 2014; McTeague et al., 2015; Li and Keil, 2023). Finally, we measured pupil re-dilation as a manipulation check, expecting greater re-dilation for the CS+ compared to the CS- because pupil re-dilation is an index of emotional arousal and sympathetic activation (Bradley et al., 2008).

Methods

Participants

Fifty (mean ± SD, 19.46 ± 1.95 years; 36 female) undergraduate students were recruited at the University of Florida in exchange for course credit. All participants provided written informed consent and reported normal or corrected-to-normal vision and a negative personal and family history of seizures. All study procedures were in accordance with the Declaration of Helsinki, and approved by the University of Florida Institutional Review Board.

Experimental design

Stimuli. Visual stimuli were developed in Matlab (MathWorks) using Psychophysics Toolbox version 3.0.15 (Brainard, 1997) and presented on a Cambridge Research Systems Display ++ monitor (1,920 × 1,080 pixels, 120 Hz refresh rate) connected to a PC running Linux Ubuntu. Each trial began with an adapter pre-stimulus period that consisted of a white fixation dot over a uniform yellow (190, 190, 0 RBG; 51.00 cd/m^2) background in Tritan conditions or a uniform black background (0, 0, 0 RBG; 0.07 cd/m^2) in luminance conditions. The adapter period preceded the onset of the flickering stimuli that consisted of oriented white gratings (255, 255, 255 RBG; 75.60 cd/m^2; 16 frames/cycle; 0.19) that were presented over the adapter period stimuli (see figure 1; Tritan grating Michelson contrast; 0.99 luminance grating Michelson contrast). There was no change in the color or luminance of the background between the adapter

period and the flickering grating presentation. The gratings flickered at a driving frequency of 7.5 Hz and exhibited a spatial frequency of 16 cycles/° with a visual angle of 3.10. The adapter period was included in the task to isolate the S-cones in the Tritan condition. The brightly colored yellow adapter field drove the medium- and long-wavelength cone responses (contributing to the luminance channels) high enough, so they were no longer reactive to changes in the visual environment (Wald, 1966). As a result, only the S-cones were sensitive to the white grating appearing over the yellow adapter (Cavanagh et al., 1992).

The unconditioned stimulus (US) was a mild electrical pulse administered using a Digitimer DS7A constant current stimulator (Hertfordshire, United Kingdom) connected to an electrode placed on the participant's non-dominant wrist. The pulse duration was 150 ms and co-terminated with the flicking grating presentation in trials where the orientation of the grating was paired with the mild electrical stimulus.

Procedure. Participants were seated about 120 cm in front of the stimulus presentation monitor in an electrically shielded, sound-attenuated room with dim lighting. Once the EEG sensor net was applied, the eye-tracking system and electrical stimulus intensity were adjusted and individually set for each participant. Before beginning the experiment, participants were provided written and verbal instructions describing that they would see a series of flickering patterns on the screen and would occasionally feel an annoying electrical stimulus. Participants were instructed that they would be asked to rate the likelihood that they would expect to feel the annoying electrical stimulus when shown each flickering pattern throughout the task. The expectancy ratings involved dragging the mouse pointer across a horizontal scale where the far left of the scale indicated "not likely that the flickering pattern was accompanied by a shock", the

middle indicated “uncertain”, and the far right indicated “certain that the flickering pattern was accompanied by a shock”.

The intensity of the electrical stimulus was determined during the shock work-up phase and was set individually for each participant prior to beginning the task. The shock work-up consisted of repeated electrical stimulus pulses that started at 0 mA and increased incrementally by 0.1 mA. After each electrical stimulus pulse, the participants rated the intensity of the stimulus using a pain scale where 0 indicated that the stimulus was not annoying, aversive, or painful and 10 indicated that the stimulus was extremely painful. The intensity was increased until the participants rated the electrical stimulus as a level 4 on the pain scale, indicating that the stimulus was highly aversive and uncomfortable, but not painful. The shock work-up consisted of two separate work-ups to a level 4 on the pain scale. The intensity level was recorded after each work-up, averaged together, and then an additional 25% of the average intensity level was added to reach the final intensity used throughout the experiment. The final intensity level was delivered to the participant immediately before beginning the experiment to ensure that it was still tolerable and not painful. If the final intensity was reported to be painful and no longer tolerable, the intensity was reduced to the mean amperage prior to the 25% increase. However, if the intensity was still intolerable then the intensity was reduced until it was tolerable for that participant. The average electrical stimulus intensity was 0.87 ± 0.68 mA ($M \pm SD$).

The task consisted of 160 trials, with 20 trials in the habituation and extinction phases and 120 trials in the acquisition phase. During the habituation phase, participants were introduced to each of the stimulus types without the presence of the mild electrical stimulus (US) and prompted to provide expectancy ratings after completing the 20 trials. In the acquisition phase, the US was introduced, and the orientation (45° or 135° clockwise tilt) of the grating

signaled the presence (CS+) or absence (CS-) of the mild electrical stimulus in the Tritan and luminance conditions. Participants provided expectancy ratings after the first 20 trials of the acquisition phase and then again after 80 trials. The orientation of the CS+ grating was counterbalanced across participants and the reinforcement rate during the acquisition phase was 100%. The extinction phase was included primarily for ethical reasons and did not include the US to reduce the association between the CS+ and the US. Participants also completed expectancy ratings after the 20 trials of extinction. Throughout the task, the occurrence of a given trial type was equiprobable and pseudo-randomized.

Data acquisition and processing

Eye-tracking. Pupil data was recorded with an EyeLink 1000 Plus system on a 16mm lens (SR Research) and sampled at 500 Hz. Offline, the continuous data was filtered using a Butterworth 6th order low-pass filter with a cutoff frequency of 0.03 Hz and segments of 600 ms pre-stimulus onset and 3800 ms post-stimulus onset were extracted from the continuous data. Segments with missing pupil data were identified and estimated using cubic interpolation. Resulting segments were averaged across conditions and baseline corrected to the average diameter of the 200 ms prior to stimulus onset.

EEG. Continuous electroencephalogram (EEG) data was recorded using a 129-electrode high-density EEG System (EGI) with Cz as the recording reference and sampled at 500 Hz. Offline data processing was completed using a custom automated EEGLAB pipeline in Matlab (Delorme and Makeig, 2004), and the code can be found here https://osf.io/yue78/ . Continuous EEG data was filtered using a 3 to 25 Hz Butterworth 4th order bandpass filter. Eye blinks were corrected using a fully automated eye correction procedure developed by Schlögl et al. (2007) and implemented using the BioSig open-source package for biomedical signal processing

(BioSig, 2005). Next, epochs of 600 ms pre-stimulus to 3800 ms post-stimulus onset were extracted from the continuous EEG data. Epochs did not include the onset of the US to preserve trials in the CS+ conditions that can be disproportionally affected by movement artifacts produced in anticipation of the US onset.

Artifact correction and rejection were carried out according to the Statistical Control of Artifacts in Dense Sensors Arrays (SCADS) procedure developed by Junghöfer et al. (2000). The SCADS approach computed a compound quality index for each participant, channel, and trial using three statistical parameters (Junghöfer et al., 2000) rectified (absolute) mean amplitude; standard deviation, maximum transient voltage change). The compound quality index was evaluated for each channel, and channels with high artifact content throughout the recording (globally bad channels) were flagged when the quality index exceeded 2.5 standard deviations above the median of the quality index. Globally bad channels were interpolated using a 2D spline interpolation method where all channels that survived artifact correction and rejection were used to estimate the values of the flagged channel. Channels at the trial level were evaluated using the same threshold for the quality index, and flagged channels were interpolated within that trial using the same spline method. Finally, trials were flagged for rejection if the compound quality index exceeded 1.25 times the median of the quality index. An average of 4% of channels in the acquisition phase were interpolated across participants (min: 0 channels; max: 15 channels), and an average of 91.60% of the total trials were retained for further analysis (Tritan CS+ = 27.64; Tritan CS- = 26.94; Luminance CS+ = 27.86; Luminance CS- = 27.48 trials on average out of 30).

The preprocessed and trial-averaged EEG data was prepared for the Hilbert transform to extract the time course of the ssVEP amplitude envelope for each condition (Figueira et al.,

2022). To this end, the EEG data was averaged across conditions for individual subjects, average referenced, and baseline corrected to the average voltage of the 200 ms prior to stimulus onset. Next, the baseline corrected data was filtered using two 9th order Butterworth filters with an upper cutoff frequency of 8 Hz and the other with a lower cutoff frequency of 7 Hz. The narrow filtering extracted the frequency that the gratings flickered at (7.5 Hz), so the results can be interpreted in a frequency band specific manner (Cohen, 2014). The filtered data was Hilbert transformed using the Matlab *hilbert.m* function to extract the time-varying estimates of phase and amplitude from the analytic signal over the entire epoch (-600 ms - 3800 ms), using the freqtag_hilbert.m function from the Matlab toolbox by Figueira et al. (2022). The Hilbert transform computes the analytic signal by doubling the positive-frequency Fourier coefficients, zeroing the negative-frequency coefficients, and taking the inverse of the Fourier transform of the doubled and zeroed Fourier coefficients (Cohen, 2014). In the time domain, the analytic signal is a phase-shifted version of the original narrowly bandpassed time series.

Statistical analyses

US expectancy ratings were analyzed using paired t-tests. The expectancy ratings after the habituation phase were examined to verify that there were no stimulus driven differences in expectancy in the absence of the US. Moreover, expectancy ratings during acquisition were analyzed to validate the aversive conditioning design, and expectancy ratings for the extinction phase were included for ethical reasons.

The ssVEP responses were analyzed using a non-parametric Bayesian approach to estimate support for the hypothesis that the ssVEP amplitude at a given time point and sensor was larger for the CS+ stimuli compared to the CS- stimuli, separately for each condition. Log10BF values were interpreted using Jeffery's scale (1961), where log10BF values between .5

to 1 indicated substantial support, log10BF values between 1 to 1.5 indicated strong support, logBF10 values between 1.5 and 2 indicated very strong support, and log10BF values greater than 2 indicated decisive support for our hypothesis. To this end, the ssVEP envelope difference across stimulus types was calculated for each sensor and time point in the acquisition phase only. As suggested by Efron (2011), evidence supporting the hypothesis was quantified by bootstrapping the condition differences (2000 iterations) as well as a null distribution (calculated through permuting condition labels within subjects, 2000 iterations). Bootstrapped distributions were generated by randomly drawing a participant's amplitude difference with replacement, for each iteration (see Ahumada et al. 2025 for a detailed description). The null distribution was generated by randomly drawing a participant's amplitude difference after randomizing the conditions with replacement, for each iteration. Bayes factors (log10BF) were computed as the posterior odds that the differences were outside the null distribution, relative to uninformative (flat) prior odds of 1. Greater evidence to support the null hypothesis (BF01) suggests that there is no difference between CS+ and CS-. Furthermore, transitive Bayes factors were computed as the ratio of Bayes factors (interpreted using Jeffrey's scale) across conditions to compare the magnitude of the Tritan and luminance conditioning effects.

Finally, pupil dilation was analyzed using a Bayesian repeated-measures ANOVA to test the hypothesis that CS+ trials would evoke greater pupil re-dilation compared to CS- trials regardless of condition.

Code accessibility

The custom preprocessing, postprocessing, and statistical analysis scripts and functions can be found at https://osf.io/yue78/.

Results

US Expectancy Ratings

Figure 2 shows the results of the paired samples t-tests computed in JASP (JASP Team, 2024) comparing the expectancy of the mild electrical stimulus when shown the CS+ or CS- grating orientations for all rating occasions across conditions (habituation, H; acquisition 1, A1; acquisition 2, A2; extinction, E). US expectancy analysis revealed that that there were no significant differences in expectancy across stimulus type for the habituation rating occasion in the luminance ($t(49) = 1.17$, $p = .250$, $d = 0.17$, paired t-test) or Tritan ($t(49) = 1.59$, $p = .119$, $d = 0.23$, paired t-test) condition. However, for each acquisition rating occasions, the CS+ trials elicited significantly higher expectancy compared to the CS- trials for both the luminance (A1: $t(49) = 7.11$, $p < .001$, $d = 1.01$, paired t-test; A2: $t(49) = 11.06$, $p < .001$, $d = 1.56$, paired t-test) and Tritan conditions (A1: $t(49) = 6.63$, $p < .001$, $d = .94$, paired t-test; A2: $t(49) = 11.13$, $p < .001$, $d = 1.57$, paired t-test). Moreover, expectancy ratings were significantly higher for CS+ trials compared to CS- trials for the extinction rating occasion in the luminance ($t(49) = 7.67$, $p < .001$, $d = 1.08$, paired t-test) and Tritan ($t(49) = 7.94$, $p < .001$, $d = 1.12$, paired t-test) conditions. Therefore, fear conditioning was successful across both experimental conditions.

Steady-state Visual Evoked Potentials

Figure 3A shows the frequency spectrum of the visuocortical activity at sensor Oz (75) in the Tritan CS+ condition across all participants in the acquisition phase. The spike in the frequency spectrum at 7.5 Hz indicates that the driving frequency was present in the spectrum. Furthermore, figure 3B shows the results of the Hilbert transform at sensor Oz (75) across participants for each trial type in each condition, indicating that the driving frequency elicited visuocortical amplification regardless of condition.

Figure 4 shows the results of the non-parametric Bayesian bootstrapped approach used to estimate support for the hypothesis that the ssVEP amplitude at a given time point and sensor was larger for the CS+, compared to the CS-, separately for the luminance and Tritan conditions. For the luminance condition, an early conditioning effect (0 ms - 1000 ms) showed decisive support for our hypothesis (log10BF > 2, peak log10BF = 2.07 at 620 ms) in a right-lateralized occipital cluster of sensors (75, 83 (O2), 84, 89, and 90; luminance O2 cluster). Moreover, for the Tritan condition, an early conditioning effect was also observed, but in a left-lateralized occipital cluster of sensors (65, 66, 69, 70 (O1), and 75; Tritan O1 cluster) and showed decisive support for our hypothesis (log10BF > 2, peak log10BF = 2.22 at 576 ms). For the Tritan condition, a late conditioning effect (1500 ms - 2500 ms) was observed in a cluster of several anterior sensors over the right and left hemispheres (29, 30, 35, 36 (C3), 80, 87, 104 (C4), and 105; Tritan anterior cluster) and showed decisive support for our hypothesis (log10BF > 2, peak log10BF = 2.10 at 2206 ms).

Figure 5 shows the Bayesian bootstrapped z-transformed conditioning effect and null distributions for sensors and time points corresponding to the clusters identified in figure 4. The early luminance distributions were computed for sensor O2 at 620 ms, the early Tritan distributions were computed for sensor O1 at 576 ms, and the late Tritan distributions were computed for sensor C4 at 1950 ms and sensor C3 at 2206 ms. The early luminance distributions at sensor O2 showed less overlap between the null and effect distributions, compared to the early Tritan distributions at sensor O1. Furthermore, the late Tritan distributions at sensor C3 showed less overlap between the null and effect distributions, compared to the late Tritan distributions at

sensor C4.

Figure 6 shows the transitive Bayes factors mapped across all sensors for the early and late time windows that were identified in figure 4. Transitive Bayes factors were computed as the ratio of the Bayes factors for the Tritan conditioning effects to the Bayes factors of the luminance conditioning effects. Therefore, negative transitive Bayes factors indicated evidence that the luminance conditioning effect was larger than the Tritan conditioning effect, and positive transitive Bayes factors indicated evidence that the Tritan conditioning effect was larger than the luminance conditioning effect at a given time point and sensor. Transitive Bayesian comparisons showed decisive evidence that the early luminance conditioning effect was larger than the early Tritan conditioning effect (0 ms - 1000 ms) in a considerable number of central and right-lateralized occipital sensors (log10BF > 2; peak log10BF = -3.13, sensor Pz; peak log10BF = -3.06, sensor 90). Furthermore, transitive Bayes factors showed decisive evidence that the early Tritan conditioning effect was larger than the early luminance conditioning effect, but in only a small number of non-adjacent left-lateralized occipital sensors 47, 52, and 65 (log10BF > 2; peak log10BF = 2.40, sensor 65). Moreover, the late Tritan conditioning effect (1500 ms - 2500 ms) persisted after transitive Bayes comparisons and showed decisive evidence in a substantial number of anterior bilateral sensors (log10BF> 2; peak log10BF = 3.37, sensor C3, left hemisphere; peak log10BF = 2.83, sensor C4, right hemisphere).

Pupil

Figure 7 shows the results of the 2 (Condition) X 2 (Stimulus type) Bayesian repeated measures ANOVA computed in JASP (JASP Team, 2024) that examined the effect of condition (luminance and Tritan) and stimulus type (CS+ and CS-) on pupil diameter in millimeters over the last two seconds of the epoch (1800 ms - 3800 ms). The results indicated that the model that

contained a main effect of Condition and Stimulus type exhibited decisive support (log10BF = 32.98), and there was no evidence of an interaction between Condition and Stimulus type. Bayesian post-hoc tests showed decisive evidence for differences in pupil diameter across luminance and Tritan conditions (log10BF = 63.20) and stimulus types (log10BF = 2.91). Pupil diameter, regardless of stimulus type, was smaller in the luminance condition (CS+, M = -0.60 mm; CS-, M = -0.66 mm) compared to the Tritan condition (CS+, M = 0.22 mm; CS-, M = 0.16 mm), and the CS+ stimuli elicited larger pupil diameters compared to the CS- stimuli regardless of condition.

Discussion

The present study investigated the contribution of the koniocellular visual pathway in aversive learning in humans. We tested the hypothesis that aversive conditioning would enhance visuocortical and sympathetic activation for threat-related stimuli in the condition where the koniocellular pathway was activated, paralleling established findings for stimuli in which the full luminance information is available. As expected, the CS+ stimuli evoked increased visuocortical responses and sympathetic activation in both the luminance and Tritan conditions, compared to the CS- stimuli. In addition, transitive Bayesian comparisons were carried out to evaluate the magnitude of the conditioning effects across the Tritan and luminance conditions. Our results showed that decisive support favored the early luminance conditioning effect over the early Tritan conditioning effect. Furthermore, decisive evidence was observed over several bilateral anterior sensors at around 1500 ms to 2500 ms post-stimulus onset, and indicated the presence of a prominent late conditioning effect in the Tritan condition only.

In line with our first hypothesis, the Tritan stimuli elicited robust ssVEP responses overall. Our results extend previous electrophysiological findings of visuocortical amplification of S-cone biasing stimuli (Cottaris and De Valois, 1998; Mullen et al., 2007, 2008; Horwitz, 2020) despite the small number of S-cone sensitive retinal ganglion cells and koniocellular cells in the koniocellular layers of the LGN (Derrington et al., 1984; Martin et al., 1997; Chatterjee and Callaway, 2003). Consistent with our second hypothesis, we observed greater visuocortical activation in response to the CS+ stimuli, compared to the CS- stimuli in both the Tritan and luminance conditions. The conditioning effects in both the luminance and Tritan conditions showed decisive support (logBF10 > 2), suggesting that activity along the koniocellular pathway participates in the representation of conditioned threat in humans.

To further elucidate the specific koniocellular contribution to aversive learning, transitive Bayes factors were computed to compare the magnitude of the conditioning effects across conditions. Transitive Bayesian comparisons showed decisive evidence that the early Tritan conditioning effect was larger than the early luminance conditioning effect in only a small number of non-adjacent left-lateralized occipital sensors. However, the comparisions showed decisive evidence that the early luminance conditioning effect was larger than the early Tritan conditioning effect in a substantial number of adjacent central and right-lateralized occipital sensors. Our findings align with aversive conditioning studies that used luminance channel biasing stimuli and observed robust visuocortical amplification of threat-related stimuli compared to safe stimuli over central and right-lateralized occipital sensors (Friedl and Keil, 2021; Stegmann et al., 2023). Furthermore, the topographies of the early conditioning effects in both conditions were consistent with the notion that early visual areas contribute to the generation of ssVEP responses (Di Russo et al., 2006).

Early visual cortex contributes to the selective amplification of aversive stimuli through the interaction between feedforward projections from V1, local inhibitory interactions, and feedback projections from high-order visual areas (Angelucci et al., 2002; Shapley et al., 2003, 2007; Keil et al., 2007). Therefore, the difference in the magnitude of the early conditioning effects across conditions could be attributed to the specific neurophysiological connections associated with each channel. Luminance channels in the human visual system are thought to consist of magnocellular and parvocellular geniculo-cortical projections to the input layer of V1 (Layer 4C, Callaway, 1998). Layer 4C receives a substantial amount of excitatory geniculo-cortical innervation (Hubel and Wiesel, 1972; Garcia-Marin et al., 2019). Conversely, the koniocellular pathway exhibits more distributed geniculo-cortical projections to the output layers of V1, including layer 1 and the CO blobs in layer 2/3 (Livingstone and Hubel, 1984; Hendry and Yoshioka, 1994; Hendry and Reid, 2000).

It has been hypothesized that the laminar layers of V1 are functionally distinct, and several studies have explored how the functional property of orientation selectivity emerges in V1 across the laminar layers (Sompolinsky and Shapley, 1997; Shapley et al., 2003; Gur et al., 2005). Ringach and colleagues (2002) provided evidence that neurons in V1 display diverse orientation selectivity contributing to broadly distributed orientation selectivity across the layers of V1. Moreover, Gur and colleagues (2005) found that the distribution of orientation tuning in V1 is not uniform, and differences in tuning could be attributed to the variability of excitatory and inhibitory mechanisms in each layer of V1. For instance, local inhibition is thought to sharpen the broadly tuned excitatory projections from the LGN and may facilitate the first stage of steady-state orientation specific responses observed over early visual areas (Shapley et al., 2003, 2007). Moreover, feedback projections from higher-order visual areas are also thought to

play a role in modulating the magnitude of the ssVEP by conveying information about arousal to early visual areas and displaying a pattern of retinotopic alignment with feedforward projections from V1 (Angelucci et al., 2002; Buffalo et al., 2010; Briggs, 2020; Li and Keil, 2023). Therefore, the differences in high-order feedback projections and local inhibitory interactions that shape the ssVEP responses in each condition may contribute to the prominence of the luminance driven early conditioning effect.

Evidence of a late anterior conditioning effect was observed in the Tritan condition at around 1500 ms to 2500 ms and showed decisive support for the hypothesis that the ssVEP responses to the Tritan CS+ stimuli were larger than the responses to the Tritan CS- stimuli. The late Tritan conditioning effect persisted after transitive Bayesian comparisons that showed decisive support over bilateral anterior sensors. Although ssVEP responses tend to emerge maximally over occipital sensors, ssVEP generation is not limited to retinotopic visual areas, and area MT also contributes to the ssVEP generation (Di Russo et al., 2006; Petro et al., 2017). Notably, the koniocellular pathway exhibits a monosynaptic geniculo-cortical projection to area MT that bypasses V1, and functional imaging has revealed that S-cone biasing stimuli elicit MT activation (Sincich et al., 2004; Mullen et al., 2008). Moreover, prior work observed that anterior ssVEP responses tend to diminish after spatial analysis was conducted (surface Laplacian), which may indicate that the sources contributing to anterior ssVEP response are deep or broad sources (Srinivasan et al., 2006). Therefore, it may be plausible that the pattern of subcortical connectivity the koniocellular pathway exhibits, involving the superior colliculus and the pulvinar nucleus, could contribute to the emergence of the robust anterior late Tritan conditioning effect. However, future investigations using neuroimaging methods with spatial

capabilities are needed to address the potential involvement of cortical, subcortical, and deep cortical structures in the late Tritan conditioning effect.

The present study extends our knowledge of the functional properties of the koniocellular visual pathway, providing evidence of the koniocellular contribution to aversive learning in humans. We replicated previous findings showing enhanced visuocortical activation in response to Tritan stimuli. Furthermore, the current findings suggest that both the koniocellular pathway and luminance-sensitive channels play a role in the visuocortical enhancement of threat signals in human visual cortex.

References

Ahumada L, Panitz C, Traiser CM, Gilbert FE, Ding M, Keil A (2025) Quantifying population-level neural tuning functions using Ricker wavelets and the Bayesian bootstrap. J Neurosci Methods 413.

Angelucci A, Levitt JB, Lund JS (2002) Anatomical origins of the classical receptive field and modulatory surround field of single neurons in macaque visual cortical area Vl. Prog Brain Res 136:373–388.

BioSig for Matlab and Octave – an open source software library for biomedical signal processing (2005).

Bradley MM, Miccoli L, Escrig MA, Lang PJ (2008) The pupil as a measure of emotional arousal and autonomic activation. Psychophysiology 45:602–607.

Brainard DH (1997) The psychophysics toolbox. Spat Vis 10:433–436.

Briggs F (2020) Role of feedback connections in central visual processing. Annu Rev Vis Sci 6:313–334.

Buffalo EA, Fries P, Landman R, Liang H, Desimone R (2010) A backward progression of attentional effects in the ventral stream. PNAS 107:361–365.

Callaway EM (1998) Local circuits in primary visual cortex of the macaque monkey. Annual Reviews Neuroscience 21:47–74.

Casagrande VA, Khaytin I, Boyd J (2007) The evolution of parallel visual pathways in the brains of primates. Primates 4:87–108.

Casagrande VA (1994) A third parallel visual pathway to primate area V1. Trends Neurosci 17:305–310.

Cavanagh P, Adelson EH, Heard P (1992) Vision with equiluminant color contrast: 2. A large-scale technique and observations. 21:219–226.

Chatterjee S, Callaway EM (2003) Parallel colour-opponent pathways to primary visual cortex. Letters to nature 426:668–671.

Cohen MX (2014). Bandpass filtering and the Hilbert transform. In: Analyzing neural time series data: Theory and practice, MIT Press.

Cottaris NP, De Valois RL (1998) Temporal dynamics of chromatic tuning in macaque primary visual cortex. Letters to Nature 395:896–900.

Dacey DM (2000) Parallel pathways for spectral coding in primate retina. Annu Rev Neurosci 23:743–775.

Delorme A, Makeig S (2004) EEGLAB: an open source toolbox for analysis of single-trial EEG dynamics including independent component analysis.

Derrington AM, Krauskopf J, Lennie P (1984) Chromatic mechanisms in lateral geniculate nucleus of macaque. Journal of Physiology 357:241–265.

Di Russo F, Pitzalis S, Aprile T, Spitoni G, Patria F, Stella A, Spinelli D, Hillyard SA (2006) Spatiotemporal analysis of the cortical sources of the steady-state visual evoked potential. Hum Brain Mapp 28:323–334.

Efron B (2011) The bootstrap and Markov-Chain Monte Carlo. J Biopharm Stat 21:1052–1062.

Figueira JSB, Kutlu E, Scott LS, Keil A (2022) The FreqTag toolbox: A principled approach to analyzing electrophysiological time series in frequency tagging paradigms. Dev Cogn Neurosci 54.

Friedl WM, Keil A (2021) Aversive conditioning of spatial position sharpens neural population-level tuning in visual cortex and selectively alters alpha-band activity. Journal of Neuroscience 41:5723–5733.

Garcia-Marin V, Kelly JG, Hawken MJ (2019) Major feedforward thalamic input into layer 4c of primary visual cortex in primate. Cerebral Cortex 29:134–149.

Gur M, Kagan I, Snodderly DM (2005) Orientation and direction selectivity of neurons in V1 of alert monkeys: Functional relationships and laminar distributions. Cerebral Cortex 15:1207–1221.

Hendry SHC, Reid RC (2000) The koniocellular pathway in primate vision. Annu Rev Neurosci 23:127–153.

Hendry SHC, Yoshioka T (1994) A neurochemically distinct third channel in the macaque dorsal lateral geniculate nucleus. Science (1979) 264:575–577.

Horwitz GD (2020) Signals related to color in the early visual cortex. Annual Review of Vision. Science 6:287–311.

Hubel DH, Wiesel TN (1972) Laminar and columnar distribution of geniculo-cortical fibers in the macaque monkey. Journal of Comparative Neurology 146:421–450.

Huo BX, Zeater N, Lin MK, Takahashi YS, Hanada M, Nagashima J, Lee BC, Hata J, Zaheer A, Grünert U, Miller MI, Rosa MGP, Okano H, Martin PR, Mitra PP (2019) Relation of koniocellular layers of dorsal lateral geniculate to inferior pulvinar nuclei in common marmosets. European Journal of Neuroscience 50:4004–4017.

JASP Team (2024). JASP (Version 0.16.3).

Jeffreys H (1961) Theory of probability. Oxford, UK: Oxford UP.

Johnson EN, Hawken MJ, Shapley R (2004) Cone inputs in macaque primary visual cortex. J Neurophysiol 91:2501–2514.

Junghöfer M, Elbert T, Tucker DM, Rockstroh B (2000) Statistical control of artifacts in dense array EEG/MEG studies. Psychophysiology 37:523–532.

Kaas JH, Lyon DC (2007) Pulvinar contributions to the dorsal and ventral streams of visual processing in primates. Brain Res Rev 55:285–296.

Keil A, Stolarova M, Moratti S, Ray WJ (2007) Adaptation in human visual cortex as a mechanism for rapid discrimination of aversive stimuli. Neuroimage 36:472–479.

Krebs RM, Woldorff MG, Tempelmann C, Bodammer N, Noesselt T, Boehler CN, Scheich H, Hopf JM, Duzel E, Heinze HJ, Schoenfeld MA (2010) High-field fMRI reveals brain activation patterns underlying saccade execution in the human superior colliculus. PLoS One 5:e8691.

Li W, Keil A (2023) Sensing fear: fast and precise threat evaluation in human sensory cortex. Trends Cogn Sci 27:341–352.

Liu X, Huang H, Snutch TP, Cao P, Wang L, Wang F (2022) The superior colliculus: Cell types, connectivity, and behavior. Neurosci Bull 38:1519–1540.

Livingstone MS, Hubel DH (1984) Anatomy and physiology of a color system in the primate visual cortex. Journal of Neuroscience 4:309–356.

Martin PR, White AJR, Goodchild AK, Wilder HD, Sefton AE (1997) Evidence that blue-on cells are part of the third geniculocortical pathway in primates. European Journal of Neuroscience 9:1536–1541.

McTeague LM, Gruss LF, Keil A (2015) Aversive learning shapes neuronal orientation tuning in human visual cortex. Nat Commun 6.

Mullen KT, Dumoulin SO, Hess RF (2008) Color responses of the human lateral geniculate nucleus: Selective amplification of S-cone signals between the lateral geniculate nucleus and primary visual cortex measured with high-field fMRI. European Journal of Neuroscience 28:1911–1923.

Mullen KT, Dumoulin SO, McMahon KL, De Zubicaray GI, Hess RF (2007) Selectivity of human retinotopic visual cortex to S-cone-opponent, L/M-cone-opponent and achromatic stimulation. European Journal of Neuroscience 25:491–502.

Nassi JJ, Callaway EM (2009) Parallel processing strategies of the primate visual system. Nat Rev Neurosci 10:360–372.

Petro NM, Forest Gruss L, Yin S, Huang H, Miskovic V, Ding M, Keil A (2017) Multimodal imaging evidence for a frontocortical modulation of visual cortex during the selective processing of conditioned threat. J Cogn Neurosci 29:953–967.

Ringach DL, Shapley RM, Hawken MJ (2002). Orientation selectivity in macaque V1: Diversity and laminar dependence. Journal of Neuroscience, 22:5639–5651.

Robinson DA (1972) Eye movements evoked by collicular stimulation in the alert monkey. Vision Res 12:1795–1808.

Schlögl A, Keinrath C, Zimmermann D, Scherer R, Leeb R, Pfurtscheller G (2007) A fully automated correction method of EOG artifacts in EEG recordings. Clinical Neurophysiology 118:98–104.

Shapley R, Hawken M, Ringach DL (2003) Dynamics of orientation selectivity in the primary visual cortex and the importance of cortical inhibition mental work and also on recent theoretical work and modeling. Neuron 38:689–699.

Shapley R, Hawken M, Xing D (2007) The dynamics of visual responses in the primary visual cortex. Prog Brain Res 165:21–32.

Sincich LC, Park KF, Wohlgemuth MJ, Horton JC (2004) Bypassing V1: A direct geniculate input to area MT. Nat Neurosci 7:1123–1128.

Sompolinsky H, Shapley R (1997) New perspectives on the mechanisms for orientation. Curr Opin Neurobiol 7:514–522.

Song I, Keil A (2014) Differential classical conditioning selectively heightens response gain of neural population activity in human visual cortex. Psychophysiology 51:1185–1194.

Sprague JM, Meikle TH (1965) The role of the superior colliculus in visually guided behavior. Exp Neurol 11:115–146.

Srinivasan R, Alouani Bibi F, Nunez PL (2006) Steady-state visual evoked potentials: distributed local sources and wave-like dynamics are sensitive to flicker frequency. Brain Topogr 18:167–187.

Stegmann Y, Andreatta M, Pauli P, Keil A, Wieser MJ (2023) Investigating sustained attention in contextual threat using steady-state VEPs evoked by flickering video stimuli. Psychophysiology 60:1.

Stepniewska I (2003) The pulvinar complex. In: The Primate Visual System, 1st ed. CRC Press.

Wald G (1966) The receptors of human color vision. Science 145:1007-1017.

Figure Captions

Figure 1 Experimental paradigm. The aversive conditioning task consisted of luminance and Tritan conditions. Trials involved adapter periods (3-7 sec) that preceded the flickering grating (7.5 Hz) and followed the grating period (4 sec). The adapter preceding the flickering grating was always a uniform black background in luminance conditions and a uniform yellow background in Tritan conditions. (A) In the habituation phase, the flickering grating was presented without any US pairings. (B) In the acquisition phase, the orientation (45° or 135°) of the flickering grating signaled the presence or absence of the US (150 ms) and was counterbalanced across participants.

Figure 2 US expectancy ratings. Mean US expectancy ratings where 0 indicated low expectancy that the flickering grating is accompanied by a shock, 5 indicated uncertainty, and 10 indicated high expectancy that the flickering grating is accompanied by a shock. The habituation and extinction phases included one rating occasion (H and E), and the acquisition phase included two rating occasions (A1, 20 trials into acqusitision; A2, 80 trials into acquisition). Within subjects paired t-tests compared the expectancy across stimulus types (CS+ and CS-) and showed that the expectancy ratings for the CS+ stimuli were significantly greater, indicating high expectancy of the mild electric shock during the acquisition and extinction rating occasions only.

Figure 3 Grand mean (N = 50) ssVEP results at sensor Oz (75). The Fourier and Hilbert transformed ssVEP results. (A) The frequency spectrum for the electrocortical responses in the Tritan CS+ condition at sensor Oz collapsed across participants. The spike at 7.5 Hz in the frequency spectrum indicates the presence of the driving frequency. (B) The results of the Hilbert transform at sensor Oz for all conditions and stimulus types collapsed across participants.

Figure 4 Effects of aversive conditioning. The condition level log10BF values for the three

clusters (sensors indicated in red) of electrodes that showed decisive support for our hypothesis that the ssVEP amplitude at a given time point and sensor was larger for the CS+, compared to the CS- regardless of condition. Log10BF values were interpreted using Jeffery's scale (1961), where log10BF values between .5 to 1 indicated substantial support, log10BF values between 1 to 1.5 indicated strong support, logBF10 values between 1.5 and 2 indicated very strong support, and log10BF values greater than 2 indicated decisive support for our hypothesis. Cluster O2 included sensors 75, 83 (O2), 84, 89, and 90; cluster O1 included sensors 65, 66, 69, 70 (O1), and 75; and the anterior cluster included sensors 29, 30, 35, 36 (C3), 80, 87, 104 (C4), and 105. The occipital topographies were plotted at the time point where the occipital clusters reached the peak logBF10 value (Tritan O1 cluster blue dashed line, peak log10BF = 2.22 at 576 ms; luminance O2 cluster black dashed line, peak log10BF = 2.07 at 620 ms). The anterior topographies were plotted at the time point where the bilateral effect emerged and also reached the peak logBF10 value (Tritan anterior cluster, first purple dashed line, log10BF = 1.84 at 1950 ms; second purple dashed line, peak log10BF = 2.10 at 2206).

Figure 5 Bayesian bootstrapped z-transformed distributions for the early and late conditioning effects. Density plots of Bayesian bootstrapped z-transformed null and conditioning effect distributions at sensors O1, O2, C3, and C4. Distributions for the early and late conditioning effects were computed at the sensor and time point corresponding to the cluster identified in figure 4: early luminance effect (sensor O2 at 620 ms), early Tritan effect (sensor O1 at 576 ms), and late Tritan effect (sensor C4 at 1950 ms; sensor C3 at 2206 ms). Distributions included 2000 draws. Note that the distributions were z-transformed together to facilitate distribution fitting, so the null-distributions are not centered around zero.

Figure 6 Transitive log10BF topographic map. Topographic map of the transitive Bayes

factors computed as the ratio of Bayes factors for the Tritan condition to Bayes factors for the luminance condition. Negative transitive Bayes factors indicated evidence that the luminance conditioning effect was larger than the Tritan conditioning effect, and positive transitive Bayes factors indicated evidence that the Tritan conditioning effect was larger than the luminance conditioning effect. Transitive Bayes factor values were also interpreted using Jeffery's scale (1961), where absolute log10BF values between .5 to 1 indicated substantial support, log10BF values between 1 to 1.5 indicated strong support, logBF10 values between 1.5 and 2 indicated very strong support, and log10BF values greater than 2 indicated decisive support for our hypothesis. An early occipital effect (0 ms - 1000 ms) showed decisive evidence that the luminance conditioning effect was larger than the early Tritan conditioning effect. A late anterior effect (1500 ms - 2500 ms) showed decisive evidence that the late Tritan conditioning effect was larger than a late luminance conditioning effect.

Figure 7 Grand mean (N = 50) pupil diameter. Changes in pupil diameter over time for each condition and stimulus type collapsed across all participants. The measurement window included in the 2 (Condition) X 2 (Stimulus) Bayesian repeated measures ANOVA was 2800 ms to 3800 ms to assess differences in pupil re-dilation.

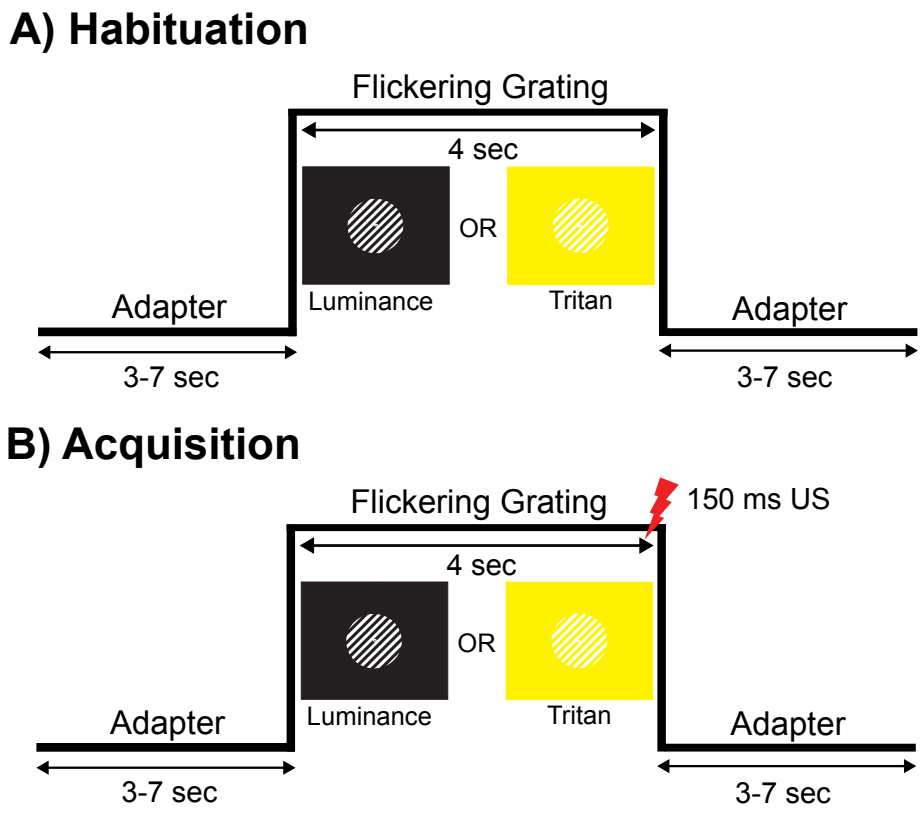

Figure 1
The aversive conditioning task consisted of luminance and Tritan conditions. Trials involved adapter periods (3-7 sec) that preceded the flickering grating (7.5 Hz) and followed the grating period (4 sec). The adapter preceding the flickering grating was always a uniform black background in luminance conditions and a uniform yellow background in Tritan conditions. (A) In the habituation phase, the flickering grating was presented without any US pairings. (B) In the acquisition phase, the orientation (45° or 135°) of the flickering grating signaled the presence or absence of the US (150 ms) and was counterbalanced across participants.

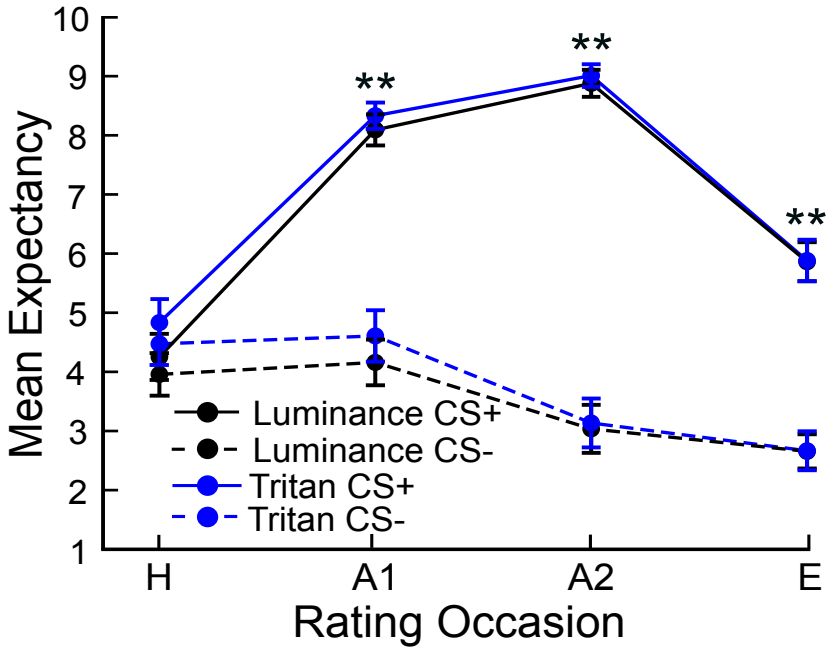

Figure 2
Mean US expectancy ratings where 0 indicated low expectancy that the flickering grating is accompanied by a shock, 5 indicated uncertainty, and 10 indicated high expectancy that the flickering grating is accompanied by a shock. The habituation and extinction phases included one rating occasion (H and E), and the acquisition phase included two rating occasions (A1, 20 trials into acqusitision; A2, 80 trials into acquisition). Within subjects paired t-tests compared the expectancy across stimulus types (CS+ and CS-) and showed that the expectancy ratings for the CS+ stimuli were significantly greater, indicating high expectancy of the mild electric shock during the acquisition and extinction rating occasions only.

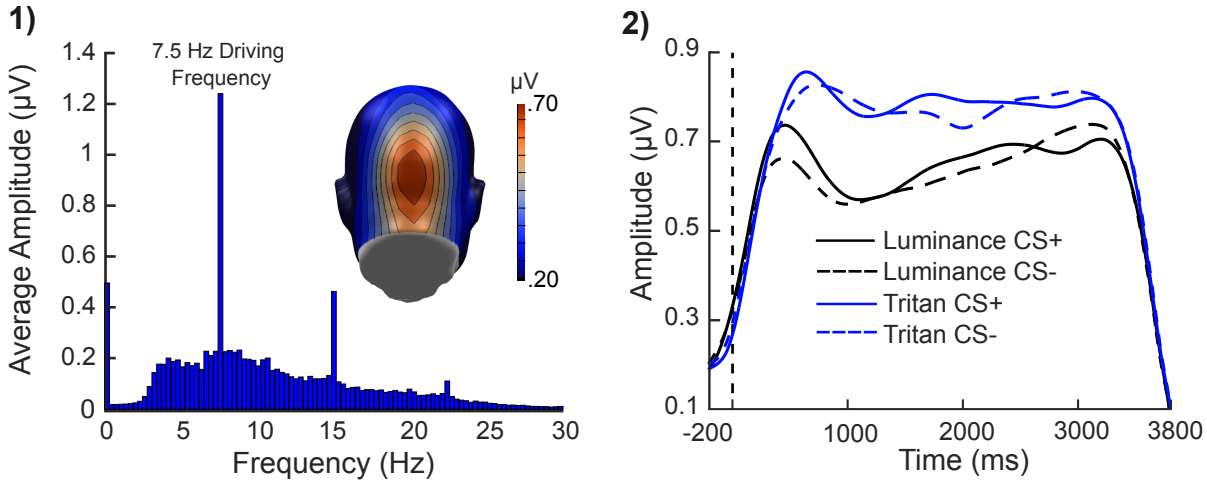

Figure 3
The Fourier and Hilbert transformed ssVEP results. (A) The frequency spectrum for the electrocortical responses in the Tritan CS+ condition at sensor Oz collapsed across participants. The spike at 7.5 Hz in the frequency spectrum indicates the presence of the driving frequency. (B) The results of the Hilbert transform at sensor Oz for all conditions and stimulus types collapsed across participants.

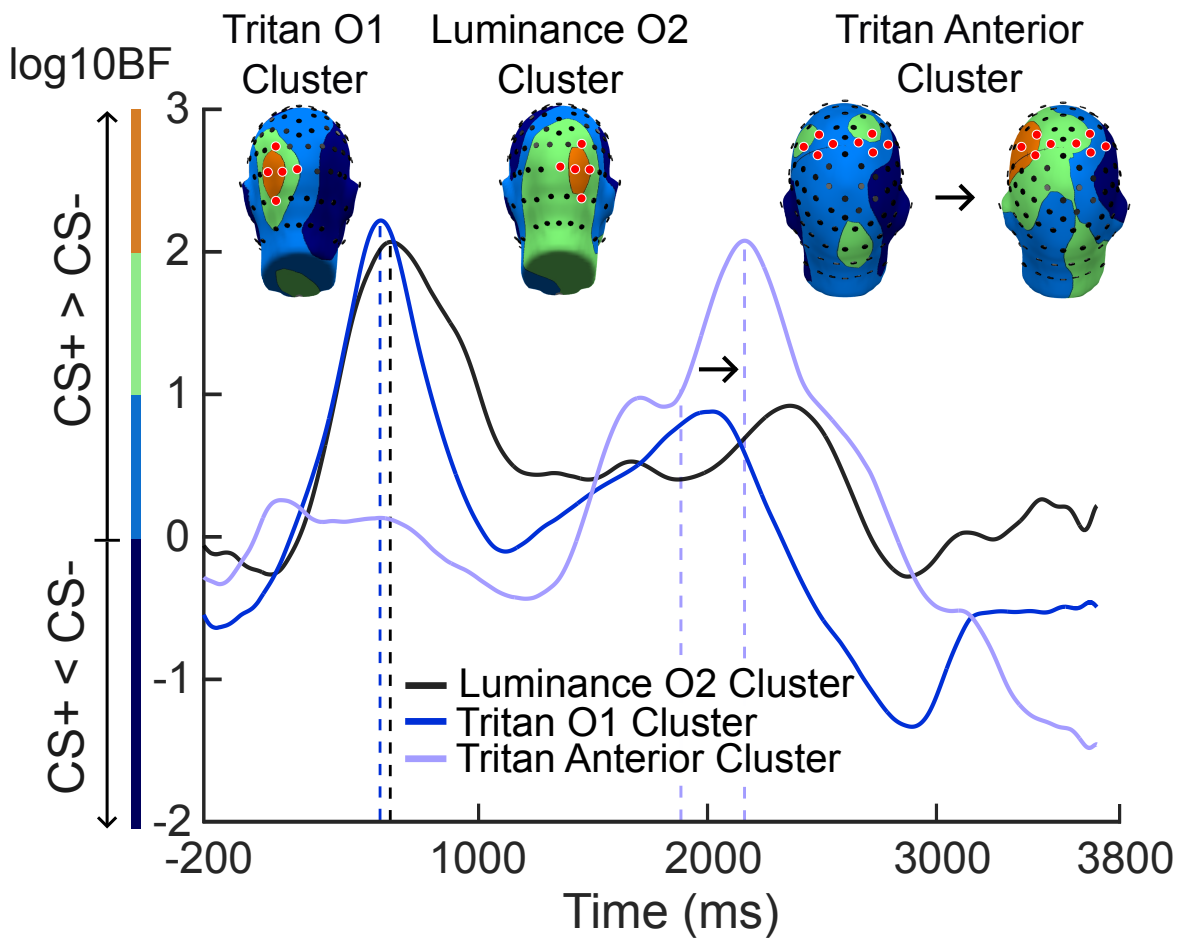

Figure 4
The condition level log10BF values for the three clusters (sensors indicated in red) of electrodes that showed decisive support for our hypothesis that the ssVEP amplitude at a given time point and sensor was larger for the CS+, compared to the CS- regardless of condition. Log10BF values were interpreted using Jeffery's scale (1961), where log10BF values between .5 to 1 indicated substantial support, log10BF values between 1 to 1.5 indicated strong support, logBF10 values between 1.5 and 2 indicated very strong support, and log10BF values greater than 2 indicated decisive support for our hypothesis. Cluster O2 included sensors 75, 83 (O2), 84, 89, and 90; cluster O1 included sensors 65, 66, 69, 70 (O1), and 75; and the anterior cluster included sensors 29, 30, 35, 36 (C3), 80, 87, 104 (C4), and 105. The occipital topographies were plotted at the time point where the occipital clusters reached the peak logBF10 value (Tritan O1 cluster blue dashed line, peak log10BF = 2.22 at 576 ms; luminance O2 cluster black dashed line, peak log10BF = 2.07 at 620 ms). The anterior topographies were plotted at the time point where the bilateral effect emerged and also reached the peak logBF10 value (Tritan anterior cluster, first purple dashed line, log10BF = 1.84 at 1950 ms; second purple dashed line, peak log10BF = 2.10 at 2206).

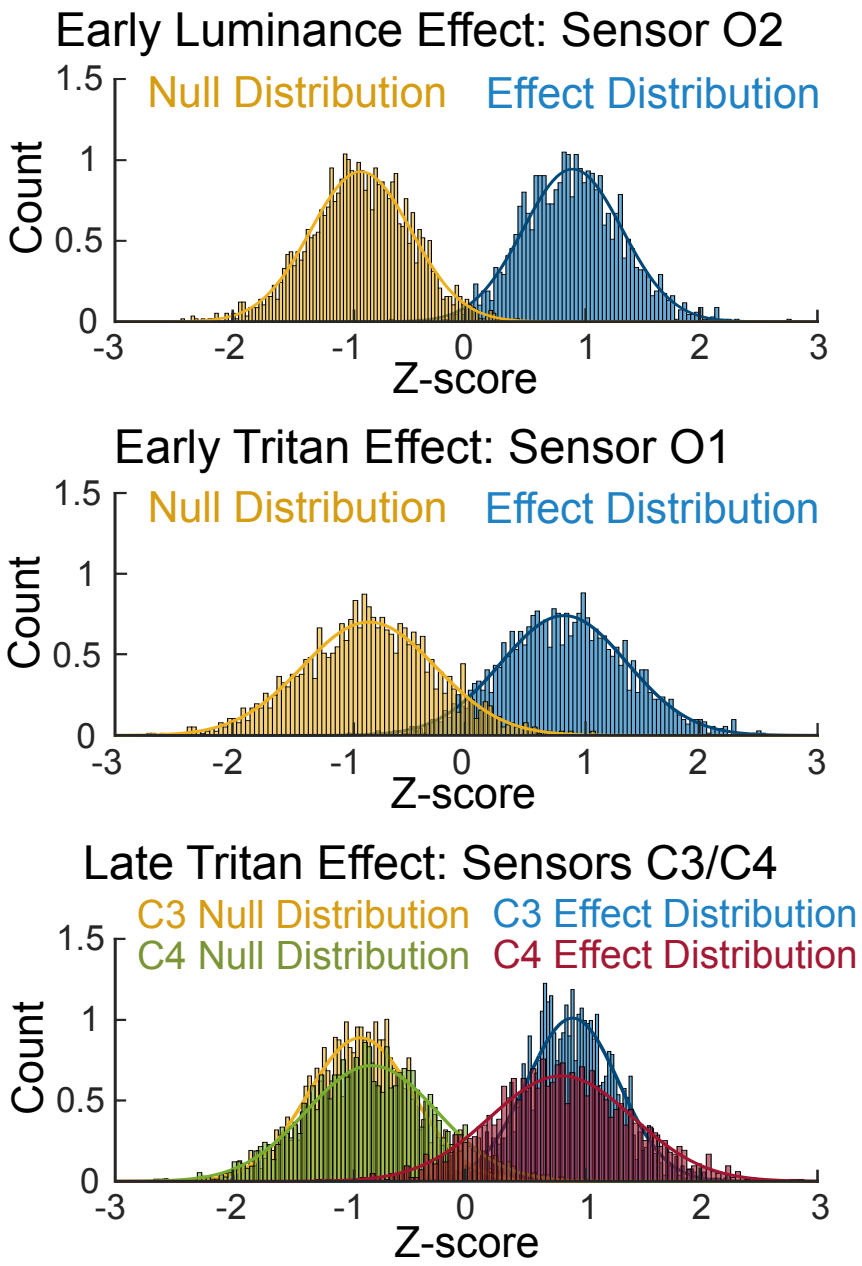

Figure 5
Density plots of Bayesian bootstrapped z-transformed null and conditioning effect distributions at sensors O1, O2, C3, and C4. Distributions for the early and late conditioning effects were computed at the sensor and time point corresponding to the cluster identified in figure 4: early luminance effect (sensor O2 at 620 ms), early Tritan effect (sensor O1 at 576 ms), and late Tritan effect (sensor C4 at 1950 ms; sensor C3 at 2206 ms). Distributions included 2000 draws. Note that the distributions were z-transformed together to facilitate distribution fitting, so the null-distributions are not centered around zero.

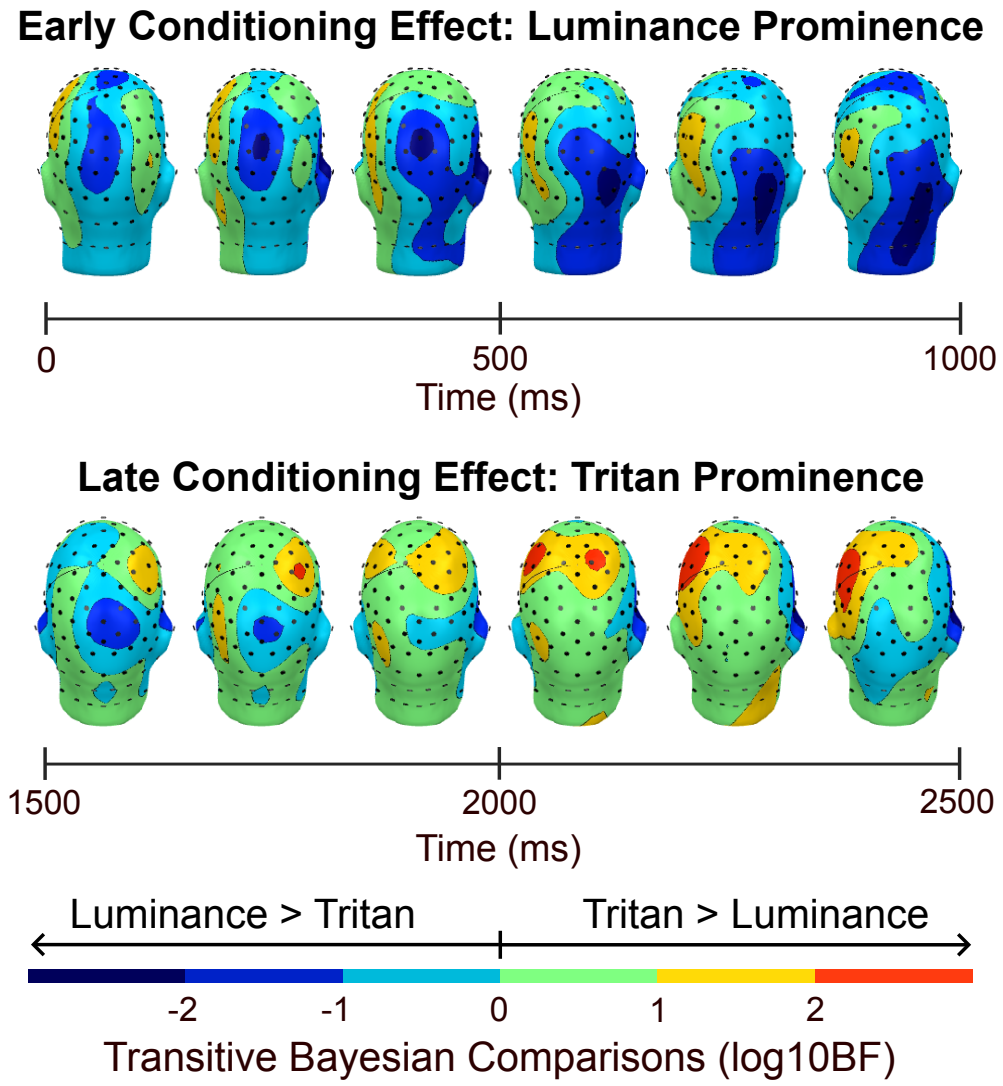

Figure 6
Topographic map of the transitive Bayes factors computed as the ratio of Bayes factors for the Tritan condition to Bayes factors for the luminance condition. Negative transitive Bayes factors indicated evidence that the luminance conditioning effect was larger than the Tritan conditioning effect, and positive transitive Bayes factors indicated evidence that the Tritan conditioning effect was larger than the luminance conditioning effect. Transitive Bayes factor values were also interpreted using Jeffery's scale (1961), where absolute log10BF values between .5 to 1 indicated substantial support, log10BF values between 1 to 1.5 indicated strong support, logBF10 values between 1.5 and 2 indicated very strong support, and log10BF values greater than 2 indicated decisive support for our hypothesis. An early occipital effect (0 ms - 1000 ms) showed decisive evidence that the luminance conditioning effect was larger than the early Tritan conditioning effect. A late anterior effect (1500 ms - 2500 ms) showed decisive evidence that the late Tritan conditioning effect was larger than a late luminance conditioning effect.

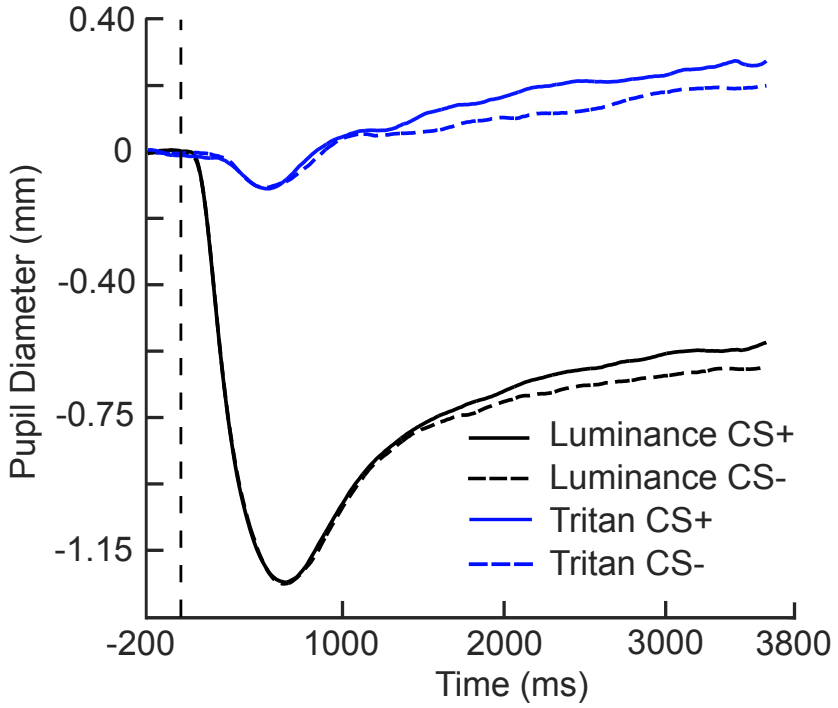

Figure 7
Changes in pupil diameter over time for each condition and stimulus type collapsed across all participants. The measurement window included in the 2 (Condition) X 2 (Stimulus) Bayesian repeated measures ANOVA was 2800 ms to 3800 ms to assess differences in pupil re-dilation.